

See discussions, stats, and author profiles for this publication at: <https://www.researchgate.net/publication/26829654>

ChemInform Abstract: Au(I)-Catalyzed Cycloisomerization Reaction of Amide- or Ester-Tethered 1,6-Enynes to Bicyclo[3.2.0]hept-6-en-2-ones

ARTICLE *in* THE JOURNAL OF ORGANIC CHEMISTRY · SEPTEMBER 2009

Impact Factor: 4.72 · DOI: 10.1021/jo901771p · Source: PubMed

CITATIONS

38

READS

13

3 AUTHORS, INCLUDING:



[Youn K. Kang](#)

Sangmyung University

34 PUBLICATIONS 616 CITATIONS

[SEE PROFILE](#)

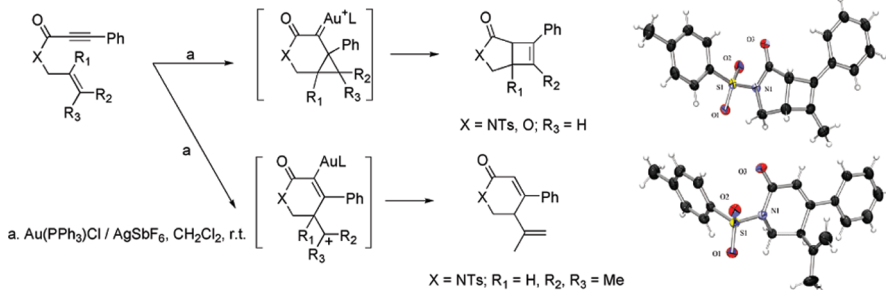
Au(I)-Catalyzed Cycloisomerization Reaction of Amide- or Ester-Tethered 1,6-Enynes to Bicyclo[3.2.0]hept-6-en-2-ones

Young Tak Lee,[†] Youn Kyung Kang,^{*,‡} and Young Keun Chung^{*,†}

[†]Intelligent Textile System Research Center, Department of Chemistry, College of Natural Sciences, Seoul National University, Seoul 151-747, Korea, and [‡]Division of Chemistry and Molecular Engineering, Department of Chemistry, College of Natural Sciences, Seoul National University, Seoul 151-747, Korea

ykchung@snu.ac.kr

Received August 25, 2009



The cycloisomerization reaction of *N*-allyl-2-(2'-arylethyne-2-yl)amides or allylic 2-alkynoates in the presence of cationic triphenylphosphinegold(I) produced bicyclo[3.2.0]hept-6-en-2-ones under mild conditions. Computational investigations with a density functional theory (DFT) revealed that a stepwise 6-*endo-dig* cyclization of 1,6-enyne systems, followed by a skeletal rearrangement to form bicyclo[3.2.0]hept-6-en-2-one species represents the most probable reaction pathway. This can be further supported by employing *N*(1',1'-dimethyl-1-propen-3-yl)-2-(1"-phenylethyne-2"-yl)amide as a substrate, which exclusively produced 4-phenyl-5-(prop-1-en-2-yl)-5,6-dihydropyridino-2(1*H*)-one unambiguously via 6-*endo-dig* cyclization. Theoretical calculations suggest both an aryl group at the terminal alkyne and a keto carbonyl at the C(5) position of the 1,6-enyne system play a complementary role for the reactivity.

Introduction

Recently, transition metal-catalyzed cycloisomerization reactions of enyne systems have been a subject of intense research due to their impact on synthetic methodologies of a range of structurally diverse products. A variety of structural frameworks can be constructed utilizing these chemical procedures by proper choice of the catalyst and the substrates.^{1–5} Among many factors that affect the reaction pathways, the formation of a stabilized carbocationic intermediate between the transition metal catalyst and the sub-

strate has been accepted as the origin for this diversity.^{2,6–10} A subtle change in the structure of the substrate, through its interplay with the catalyst system, modulates the reactivity of the system and thus leads to different reaction pathways.^{11,12}

In the electrophilic transition metal-catalyzed cycloisomerization reaction of enynes, the formation of cyclobutenes is quite limited^{13–19} although it has been considered one of the

*To whom correspondence should be addressed. Y.K.C.: phone (+82) 2-880-6662; fax (+82) 2-889-0310.

- (1) Lloyd-Jones, G. C. *Org. Biomol. Chem.* **2003**, *1*, 215–236.
- (2) Echavarren, A. M.; Nevado, C. *Chem. Soc. Rev.* **2004**, *33*, 431–436.
- (3) Bruneau, C. *Angew. Chem., Int. Ed.* **2005**, *44*, 2328–2334.
- (4) Diver, S. T.; Giessert, A. *J. Chem. Rev.* **2004**, *104*, 1317–1382.
- (5) Ma, S. M.; Yu, S. C.; Gu, Z. H. *Angew. Chem., Int. Ed.* **2006**, *45*, 200–203.

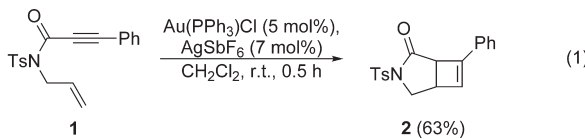
- (6) Furstner, A.; Szillat, H.; Gabor, B.; Mynott, R. *J. Am. Chem. Soc.* **1998**, *120*, 8305–8314.
- (7) Aubert, C.; Buisine, O.; Malacria, M. *Chem. Rev.* **2002**, *102*, 813–834.
- (8) Mendez, M.; Echavarren, A. M. *Eur. J. Org. Chem.* **2002**, *102*, 15–28.
- (9) Furstner, A. *Angew. Chem., Int. Ed.* **2003**, *42*, 3582–3603.
- (10) Soriano, E.; Ballesteros, P.; Marco-Contelles, J. *J. Org. Chem.* **2004**, *69*, 8018–8023.
- (11) Kim, S. M.; Lee, S. I.; Chung, Y. K. *Org. Lett.* **2006**, *8*, 5425–5427.
- (12) Lee, S. I.; Kim, S. M.; Choi, M. R.; Kim, S. Y.; Chung, Y. K.; Han, W. S.; Kang, S. O. *J. Org. Chem.* **2006**, *71*, 9366–9372.
- (13) Marion, F.; Coulomb, J.; Courillon, C.; Fensterbank, L.; Malacria, M. *Org. Lett.* **2004**, *6*, 1509–1511.

accessible products.^{6,20–27} Since there are a handful of precedents for the synthesis of cyclobutenes,^{28–35} finding a synthetic protocol selectively producing this structural motif is still challenging.

While we were studying the Au(I)-catalyzed cycloisomerization reactions of heteroatom-tethered 1,6-enynes, we found that the introduction of a keto carbonyl at the C(5) position could alter the reaction pathway from its nonketo analogues giving rise to the formation of bicyclobutenes instead of many other cycloisomerization products such as 1,3-diene derivatives or cyclopropanated compounds. Herein, we report our results along with the theoretical rationale for the observed selectivity through a DFT calculation.

Results and Discussions

Synthesis of the Bicyclo[3.2.0]hept-6-en-2-one System from Amide- or Ester-Tethered 1,6-Enynes. A cycloisomerization reaction of *N*-allyl-2-alkynylamide (**1**) in the presence of $\text{Au}(\text{PPh}_3)^+$ (generated from a reaction of $[\text{Au}(\text{PPh}_3)\text{Cl}]$ (5 mol %) with AgSbF_6 (7 mol %)) was studied initially (eq 1). The reaction went to completion within 30 min at room temperature. A bicyclobutene compound (**2**) was isolated in 63% yield. When the same substrate was reacted with PtCl_2 , on the contrary, no reaction was observed.



Considering the fact that a similar type of substrate with a simple NTs-tether (**3**) gave rise to a bicyclo[4.1.0]hept-4-ene

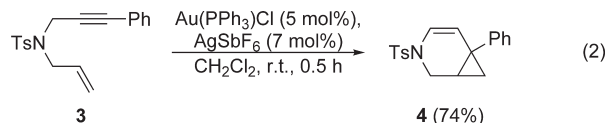
- (14) Nieto-Oberhuber, C.; Lopez, S.; Echavarren, A. M. *J. Am. Chem. Soc.* **2005**, *127*, 6178–6179.
- (15) Furstner, A.; Davies, P. W.; Gress, T. *J. Am. Chem. Soc.* **2005**, *127*, 8244–8245.
- (16) Matsuda, T.; Kadowaki, S.; Goya, T.; Murakami, M. *Synlett* **2006**, 575–578.
- (17) Mezailles, N.; Ricard, L.; Gagosc, F. *Org. Lett.* **2005**, *7*, 4133–4136.
- (18) Couty, S.; Meyer, C.; Cossy, J. *Angew. Chem., Int. Ed.* **2006**, *45*, 6726–6730.
- (19) Michelet, V.; Toullec, P. Y.; Genet, J. P. *Angew. Chem., Int. Ed.* **2008**, *47*, 4268–4315.
- (20) Trost, B. M.; Tanoury, G. J. *J. Am. Chem. Soc.* **1988**, *110*, 1636–1638.
- (21) Trost, B. M.; Trost, M. K. *Tetrahedron Lett.* **1991**, *32*, 3647–3650.
- (22) Trost, B. M.; Doherty, G. A. *J. Am. Chem. Soc.* **2000**, *122*, 3801–3810.
- (23) Furstner, A.; Szillat, H.; Stelzer, F. *J. Am. Chem. Soc.* **2000**, *122*, 6785–6786.
- (24) Furstner, A.; Stelzer, F.; Szillat, H. *J. Am. Chem. Soc.* **2001**, *123*, 11863–11869.
- (25) Chatani, N.; Inoue, H.; Morimoto, T.; Muto, T.; Murai, S. *J. Org. Chem.* **2001**, *66*, 4433–4436.
- (26) Chatani, N.; Inoue, H.; Kotsuma, T.; Murai, S. *J. Am. Chem. Soc.* **2002**, *124*, 10294–10295.
- (27) Jimenez-Nunez, E.; Echavarren, A. M. *Chem. Rev.* **2008**, *108*, 3326–3350.
- (28) Inanaga, K.; Takasu, K.; Ihara, M. *J. Am. Chem. Soc.* **2005**, *127*, 3668–3669.
- (29) Liu, Y. H.; Liu, M. N.; Song, Z. Q. *J. Am. Chem. Soc.* **2005**, *127*, 3662–3663.
- (30) Canales, E.; Corey, E. J. *J. Am. Chem. Soc.* **2007**, *129*, 12686–12687.
- (31) Shi, M.; Liu, L. P.; Tang, J. *J. Am. Chem. Soc.* **2006**, *128*, 7430–7431.
- (32) Furstner, A.; Aissa, C. *J. Am. Chem. Soc.* **2006**, *128*, 6306–6307.
- (33) Tian, G. Q.; Yuan, Z. L.; Zhu, Z. B.; Shi, M. *Chem. Commun.* **2008**, 2668–2670.
- (34) Xu, H. D.; Zhang, W.; Shu, D. X.; Werness, J. B.; Tang, W. P. *Angew. Chem., Int. Ed.* **2008**, *47*, 8933–8936.
- (35) Nieto-Oberhuber, C.; Perez-Galan, P.; Herrero-Gomez, E.; Lauterbach, T.; Rodriguez, C.; Lopez, S.; Bour, C.; Rosellon, A.; Cardenas, D. J. *J. Am. Chem. Soc.* **2008**, *130*, 269–279.

SCHEME 1. Transition Metal-Catalyzed Cycloisomerization of Allylpropargylmalonates

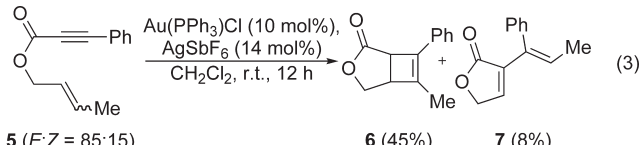
Cat	R ¹	R ²	Ar	Yield(%)
PtCl ₂	Et	H	C ₆ H ₅	24 ^a
PtCl ₂	Et	H	4-MeOC ₆ H ₄	58 ^a
Au(PPh ₃) ⁺ NTf ₂ ⁻	Me	Me	C ₆ H ₅	94 ^b

^aReference 22. ^bReference 25.

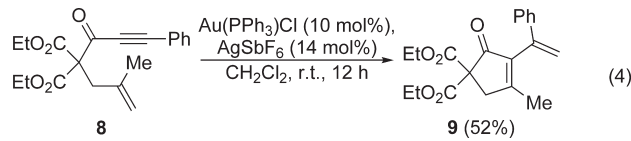
derivative (**4**) under the conditions exerted by the PtCl_2 ¹⁵ or by the $\text{Au}(\text{PPh}_3)^+$ catalysts (eq 2),³⁶ the apparent difference observed in this result clearly showed that the introduction of the keto carbonyl group at the C(5) position of the 1,6-ynye substrate completely changed the reaction pathway.



Encouraged by this result, we attempted to probe whether this chemistry can be expanded to other 1,6-ynye systems (eq 3). In the case of allylic 2-alkynoate (**5**), the reaction was rather inefficient; the cyclobutene derivative (**6**) was obtained in only 45% yield even with an increased amount of the catalyst (10 mol %) and a prolonged reaction time (12 h). Moreover, a 1,3-diene compound (**7**) was also produced in 8% yield.



Enynes with a carbon tether are known to give bicyclic cyclobutenes in platinum- or gold(I)-catalyzed cycloisomerization reactions (Scheme 1).^{14,17} However, when a keto carbonyl was introduced to a carbon tethered 1,6-ynye system, a corresponding cyclobutene was not produced at all (eq 4). Instead, a 1,3-diene compound was obtained in 52% yield.



Knowing that the formation of cyclobutenes by the Au(I)-catalyzed cycloisomerization reaction is confined only to the amide- and ester-tethered 1,6-ynye systems, we further screened the reaction with various substrates. The results are compiled in Table 1. The introduction of a mono substitution to the alkene in the enyne substrate did not change the reaction pathway. The treatment of amide-tethered enynes **10** and **12** with a methyl group at the alkene group (entries 1 and 2) led to the isolation of the corresponding

(36) Lee, S. I.; Kim, S. M.; Kim, S. Y.; Chung, Y. K. *Synlett* **2006**, 2256–2260.

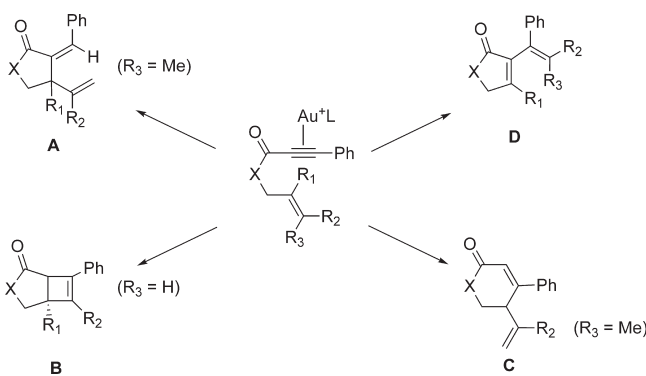
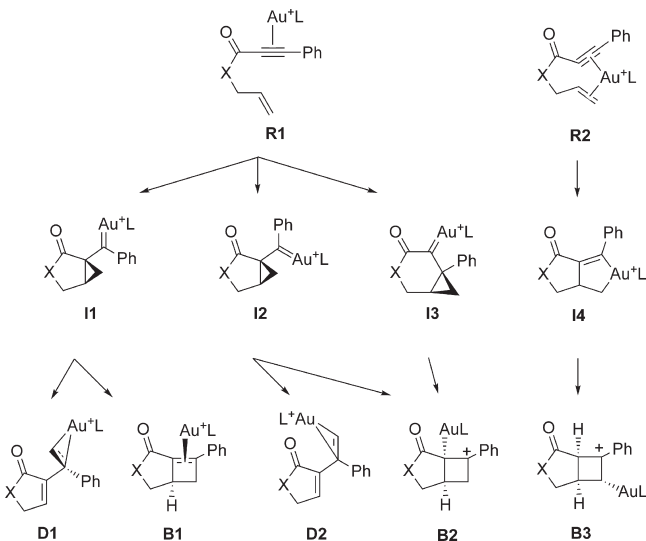
TABLE 1. Au(I)-Catalyzed Cycloisomerization Reactions of Amide- or Ester-Tethered 1,6-Enynes^a

entry	substrate	product	yield (%) ^b
1 ^c	10	11	77
2 ^c	12	13	73
3	14 (E/Z = 80:20) (E/Z = 85:15)	15	72 ^d
4	17	18	74
5	19	20	70
6	21 (E/Z = 100:0)	22	83
7	23 (E/Z = 100:0)	24	85
8 ^c	25	26	91
9	27	28	87
10	29	30	82

^a0.5 mmol of a reactant was reacted with 10 mol % of [Au(PPh₃)₃]SbF₆ in CH₂Cl₂ at room temperature for 12 h. ^bIsolated yields. ^c0.5 mmol of a reactant was reacted with 5 mol % of [Au(PPh₃)₃]SbF₆ in CH₂Cl₂ at room temperature for 0.5 h. ^dA 1,3-diene (**16**) obtained in 7% yield.

cyclobutene derivatives **11** and **13** in 77% and 73% yields, respectively. The formation of **13** was confirmed by X-ray diffraction analysis (see the SI). In the same way, ester-tethered enynes (entries 3–7) gave cyclobutenes in 70–85% yields. It should be noted that the concomitant formation of 1,3-diene (7%) in addition to the cyclobutene was observed when substrate **14** was employed (entry 3) as in the case of eq 4. The use of cyclohexenyl alkynes (entries 8–10) led to the isolation of 4,5,6-tricyclic cyclobutene compounds in 82–91% yield.

Proposed Mechanisms. The studies of the Au(I)-catalyzed cycloisomerization reaction of 1,6-enyne systems are documented in a number of reviews.^{7,37,38} Especially its mechanistic investigation via DFT calculation has been well studied by the Echavarren group.^{19,35,39,40} While there have been a number of mechanistic suggestions for the formation of cyclobutenes by transition metal-catalyzed cycloisomerization reactions, which

SCHEME 2. Proposed Au(I)-Catalyzed Cycloisomerization Reactions of Amide- or Ester-Tethered 1,6-Enynes**SCHEME 3.** Reaction Flow Chart of Au(I)-Catalyzed Cycloisomerization Reactions of Amide- or Ester-Tethered 1,6-Enynes Prepared for the DFT Computational Study

include the involvement of the cyclopropyl metal carbenes prepared via 5-exo^{26,40,41} or 6-endo-cyclization mode.¹⁵ Echavarren et al. reported that the former is favorable for carbon tethered 1,6- or 1,7-ene systems.^{39,40} Given their established framework as a benchmark, we propose plausible reactions in Scheme 2.

As mentioned by Echavarren in his recent review,²⁵ all the results of gold(I)-catalyzed cycloisomerization reactions of enyne systems reported to date can be explained in terms of a selective activation of the alkyne by gold(I) although gold(I)–alkene complexes are likely formed in equilibrium with the gold(I)–alkyne ones.²⁷ Under this scope, reactions starting from gold(I)–alkene are not considered in this work. The mechanism toward product **A**, which can be formed by an Alder-ene cycloisomerization, is also precluded given the fact that both amide- and ester-tethered 1,6-enynes with methyl group at the terminal alkene (entries 2, 3, 6, and 7 in Table 1) did not produce this type of products at all (Scheme 2). Thus our mechanistic investigation will be focused on products **B** and **D**.⁴² The corresponding reaction flowchart covered by

(37) Hashmi, A. S. K. *Chem. Rev.* **2007**, *107*, 3180–3211.

(38) Zhang, L. M.; Sun, J. W.; Kozmin, S. A. *Adv. Synth. Catal.* **2006**, *348*, 2271–2296.

(39) Nieto-Oberhuber, C.; Munoz, M. P.; Bunuel, E.; Nevado, C.; Cardenas, D. J.; Echavarren, A. M. *Angew. Chem., Int. Ed.* **2004**, *43*, 2402–2406.

(40) Nieto-Oberhuber, C.; Lopez, S.; Munoz, M. P.; Cardenas, D. J.; Bunuel, E.; Nevado, C.; Echavarren, A. M. *Angew. Chem., Int. Ed.* **2005**, *44*, 6146–6148.

(41) Peppers, B. P.; Diver, S. T. *J. Am. Chem. Soc.* **2004**, *126*, 9524–9525.

(42) The synthesis of C-type compound will be discussed in later part of this paper.

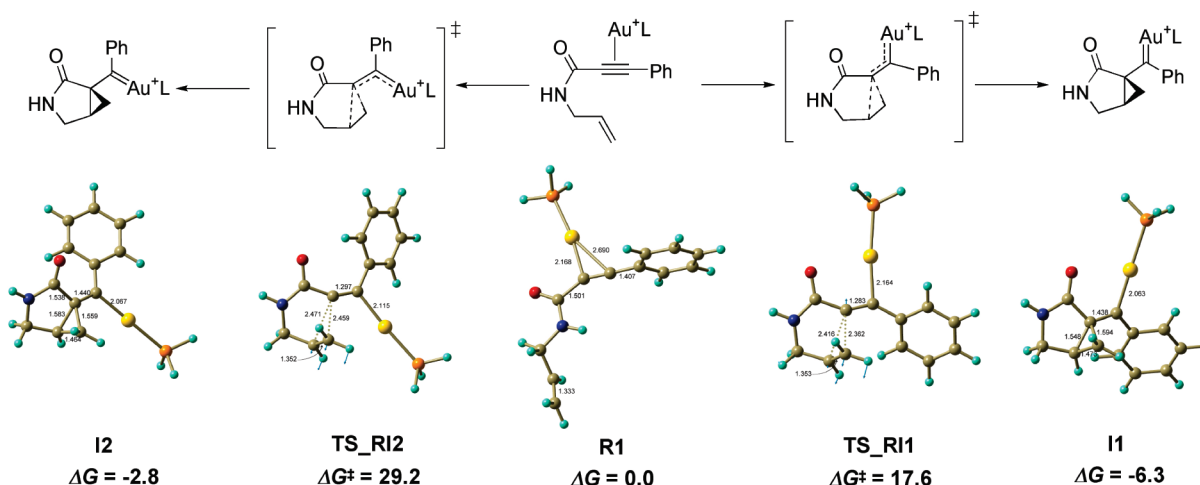


FIGURE 1. Reaction diagram of 5-exo-syn- (to the left) and 5-exo-anti-cyclization (to the right) of amide-tethered 6-phenyl-1,6-ene. Geometries of stationary points are optimized structures via DFT at the B3LYP/6-31G(d) and LANL2DZ levels. Zero point energy (ZPE) corrected free energies are given in kcal/mol. Arrows (sky blue) in the transition state geometries indicate displacement vectors of vibrational mode possessing an imaginary frequency.

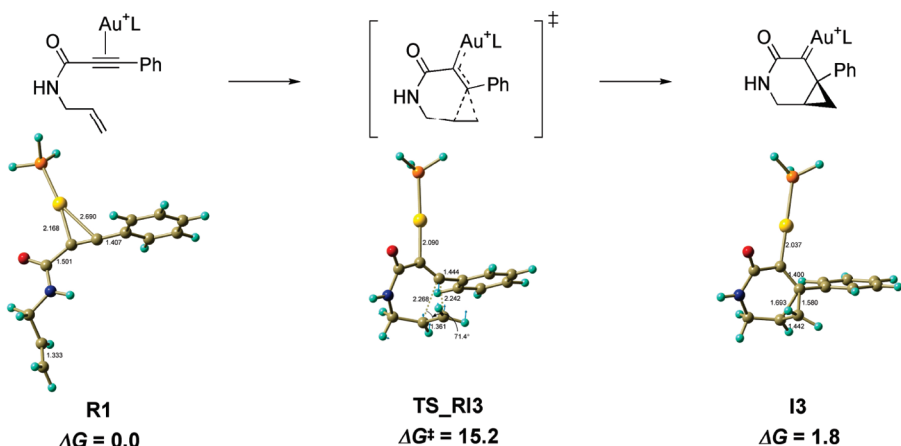


FIGURE 2. Reaction diagram of 6-endo-cyclization of amide-tethered 6-phenyl-1,6-ene. Geometries of stationary points are optimized structures via DFT at the B3LYP/6-31G(d) and LANL2DZ levels. ZPE corrected free energies are given in kcal/mol. Arrows (sky blue) in the transition state geometries indicate displacement vectors of vibrational mode possessing an imaginary frequency.

computational study in this work is shown in Scheme 3. It should be addressed that the reactant state in which phosphinegold(I) is bound to both alkyne and alkene (**R2**) is also considered to probe the pathway involving metallocycle intermediate (**I4**). Besides two forms of cyclopropyl metal carbene complexes, **I1** (via 5-exo-anti-cyclization) and **I3** (via 6-endo-cyclization), the intermediate **I2** (via 5-exo-syn-cyclization) is also considered because reaction barriers for both a 5-exo-cyclization step (**R1_I1** or **I2**) and its further rearrangement to a cyclobutene (**I1_B1** or **I2_B2**) can be largely affected by the relative orientation of a phosphinegold(I) moiety in the cyclopropyl metal carbene complex.⁴⁰ Three types of cyclobutenes and two types of dienes are corresponding products derived from **I1–I4** intermediates.

Mechanisms from R to I. The energetics and the structures of each stationary point for the formation of cyclopropyl metal carbene intermediates are illustrated in Figures 1 (5-exo) and 2 (6-endo). Similar to the case of Echavarren et al., in which either a keto carbonyl group or a phenyl ring at the C(5) and C(7) atoms, respectively, were not introduced, the free

energy level of **I1** ($\Delta G = -6.3$ kcal/mol) is slightly more stable than that of **I2** ($\Delta G = -2.8$ kcal/mol).³⁹ However, in contrast to Echavarren's case, where the energy level of 6-endo-cyclization product is residing below those of 5-exo-ones, **I3** in this work becomes destabilized ($\Delta G = 1.8$ kcal/mol) and thus lies above the level of **I2** by 4.6 kcal/mol. This reversion of energy order between **I2** and **I3** leads the major difference of mechanistic pathway for the formation of cyclobutene, which will be discussed in the next part of this paper.

In Echavarren's work, the transition state for the 5-exo-anti-process served as the lowest reaction barrier with near zero activation energy. In our result, however, the free energy barrier for the 6-endo-cyclization (**TS_RI3**) was slightly lower ($\Delta G^\ddagger = 15.2$ kcal/mol) than that for the 5-exo-anti-one (**TS_RI1**, $\Delta G^\ddagger = 17.6$ kcal/mol). **TS_RI2** has a much higher free energy barrier than the other two ($\Delta G^\ddagger = 29.2$ kcal/mol); the first step of the reaction is thus most likely toward **I3** or **I1** and the possibility of its being toward **I2** can be practically excluded.

Mechanisms toward Cyclobutenes or 1,3-Dienes. The transformations from cyclopropyl metal carbene intermediates to

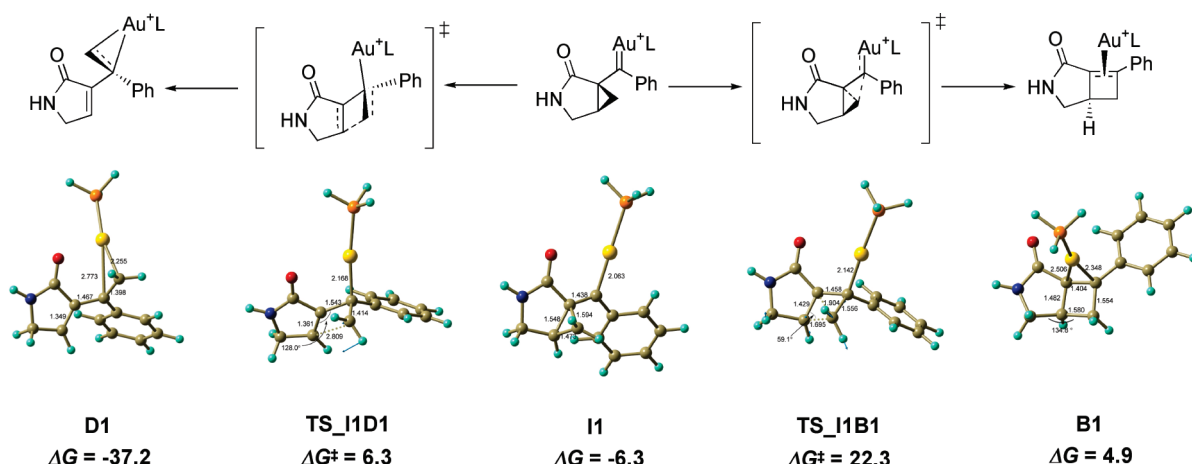


FIGURE 3. Reaction diagram of transformations from the cyclopropyl metal carbene intermediate (**I1**) to the 1,3-diene (**D1**, to the left) and cyclobutene (**B1**, to the right). Geometries of stationary points are optimized structures via DFT at the B3LYP/6-31G(d) and LANL2DZ levels. ZPE corrected free energies are given in kcal/mol. Arrows (sky blue) in the transition state geometries indicate displacement vectors of vibrational mode possessing an imaginary frequency.

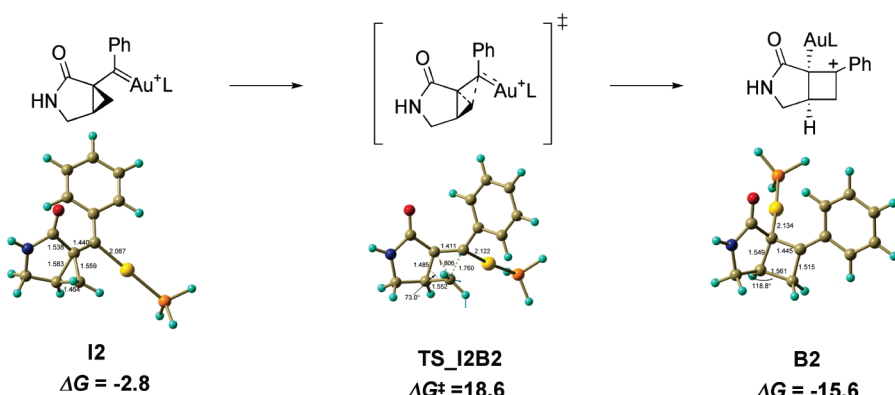


FIGURE 4. Reaction diagram of the transformation from the cyclopropyl metal carbene intermediate (**I2**) to the cyclobutene (**B2**). Geometries of stationary points are optimized structures via DFT at the B3LYP/6-31G(d) and LANL2DZ levels. ZPE corrected free energies are given in kcal/mol. Arrows (sky blue) in the transition state geometries indicate displacement vectors of vibrational mode possessing an imaginary frequency.

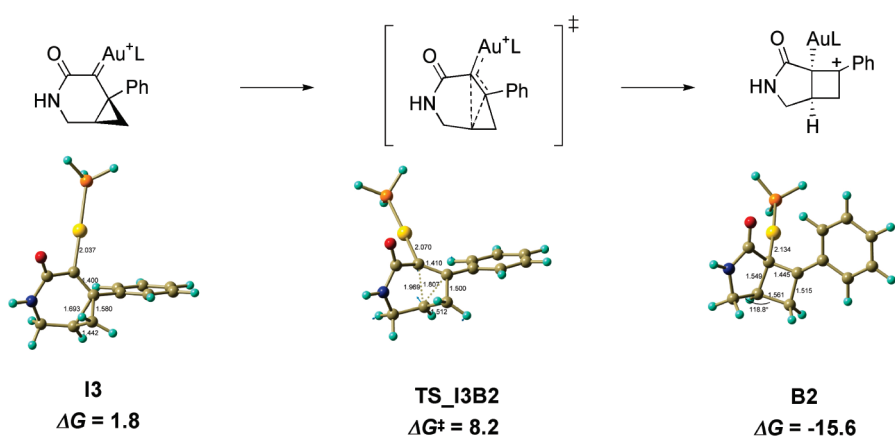


FIGURE 5. Reaction diagram of the transformation from the cyclopropyl metal carbene intermediate (**I3**) to the cyclobutene (**B3**). Geometries of stationary points are optimized structures via DFT at the B3LYP/6-31G(d) and LANL2DZ levels. ZPE corrected free energies are given in kcal/mol. Arrows (sky blue) in the transition state geometries indicate displacement vectors of vibrational mode possessing an imaginary frequency.

their corresponding cyclobutene or 1,3-diene complexes are illustrated in Figures 3–5. The 5-exo-anti-product **I1** could

evolve to either cyclobutene (**B1**) via **TS_I1B1** or 1,3-diene (**D1**) via **TS_I1D1** (Figure 3). The structure of **TS_I1B1**

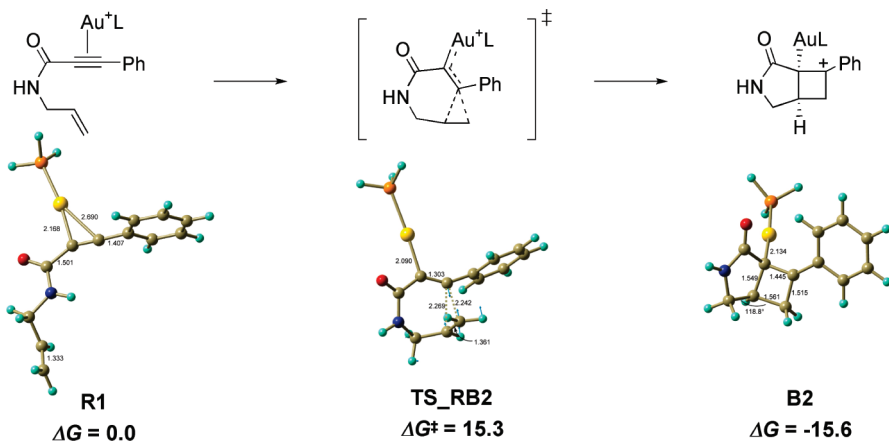


FIGURE 6. Reaction diagram of the direct transformation from the reactant (**R1**) to the cyclobutene (**B2**). Geometries of stationary points are optimized structures via DFT at the B3LYP/6-31G(d) and LANL2DZ levels. ZPE corrected free energies are given in kcal/mol. Arrows (sky blue) in the transition state geometries indicate displacement vectors of vibrational mode possessing an imaginary frequency.

clearly shows the smooth ring expansion process from **I1** to **B1** exhibiting the lengthened (1.904 Å) and the shortened (1.556 Å) bond distances for the cleaved (C(1)–C(6)) and the newly formed (C(1)–C(7)), respectively. The structure of **TS_I1D1** seems to be similar to that of **TS_I1B1** yet more close to that of the 1,3-diene product. The bond distances of C(2)–C(6) and C(1)–C(7) are 1.361 and 1.414 Å, respectively, indicating apparent double bond characters. A notable difference from **TS_I1B1** is the C(1)–C(2) distance (2.809 Å), showing there is no more bonding character between these two atoms. The free energy barrier from **I1** to **D1** ($\Delta G^\ddagger = 6.3$ kcal/mol) is ca. 16 kcal/mol lower than that to **B1** ($\Delta G^\ddagger = 22.3$ kcal/mol). Thus the evolution from **I1** is most likely to the 1,3-diene product.

On the other hand, the 5-*exo*-*syn*-product **I2** gave rise to the formation of cyclobutene (**B2**) via **TS_I2B2** with the activation free energy of 21.4 kcal/mol (Figure 4). In spite of extensive computational searching, however, we were not able to find the transition state for the **I2_D2** process.

Interestingly, the 6-*endo*-cyclization product **I3** did evolve to the cyclobutene (**B2**) through **TS_I3B2**⁴³ (Figure 5). The structure of the transition state displays the bond cleavage between C(2) and C(7) (1.807 Å) with the concomitant bond formation between C(2) and C(6) (1.969 Å). The free energy level of **TS_I3B2** was 8.2 kcal/mol, which is slightly higher than that of **TS_I1D1**. However, the activation free energy for this process was only 6.4 kcal/mol due to the highly destabilized **I3** state as previously mentioned. Considering the fact that the magnitude of the activation barrier of this process is the smallest among three processes (**I1_TS_I1B1_B1**, **I2_TS_I2B2_B2**, and **I3_TS_I3B2_B2**) and **TS_RI3** served as the lowest barrier from the reactant state (**R1**) to the cyclopropyl metal carbene intermediates, the most probable reaction pathway for the formation of cyclobutene is thus the **R1_I3_B2** route. Moreover the activation barrier for the **I3_B2** process is much smaller than that for the **I1_D1** one demonstrating that the formation of cyclobutene is more favorable than that of 1,3-diene.

Mechanism via Direct Transformation from R1 to B2: The Possibility of Reaction Pathway Bifurcation. During the

computational investigation, we found the transition state that directly connects **R1** and **B2**. Interestingly, the structure, the energy level, the magnitude of the imaginary vibrational frequency, as well as the vibrational mode of this transition state (**TS_RB2**) were virtually identical with those of **TS_RI3** implying that the reaction pathway bifurcation may possibly be involved in this state⁴⁴ (Figure 6).

As illustrated in Figures 5 and 6, the displacement vectors for the vibrational mode possessing imaginary frequency of this transition state demonstrate that the C(7) atom appeared to fluctuate on the C(1)–C(2) ethylene plane. When two units (C(7) and C(1)–C(2) double bond) approach each other, either C(1)–C(2)–C(7) cyclopropane or C(1)–C(2)–C(6)–C(7) cyclobutene is likely to form. Due to this additional pathway, the possibility for the formation of cyclobutene product is augmented. As a result, the competition between the pathway toward the 1,3-diene and that toward the cyclobutene ends up with the victory of the latter.

Mechanism through Metallacycle Intermediate. Although oxidative additions involving phosphinegold(I) complexes are known to be difficult,⁴⁵ it was possible to locate the metallacycle intermediate **I4** in the computational calculation (Figure 7). This state is most likely derived from **R2** in which phosphinegold(I) binds to both alkyne and alkene since, as we already confirmed, **R1** gave rise to cyclopropyl metal carbene intermediates rather than a metallacycle. The structure of **R2** exhibits that the Au–alkyne distance (Au–C(6), 2.295 Å) is shorter than the Au–alkene one (Au–C(1), 2.457 Å or Au–C(2), 2.486 Å) assuring the alkynophilicity of gold. Bond distances of C(1)–C(2) and C(6)–C(7) are 1.368 and 1.248 Å, indicating that the double and the triple bond characters for the former and the latter, respectively, still persist. In metallacycle **I4**, these distances are lengthened to 1.521 and 1.335 Å exhibiting that those two bonds are turning into the single and the double bonds, respectively.

The structure of the transition state **TS_R2I4** suggests that the formation of metallacycle is stepwise rather than

(44) Ess, D. H.; Wheeler, S. E.; Iafe, R. G.; Xu, L.; Celebi-Olcum, N.; Houk, K. N. *Angew. Chem., Int. Ed.* **2008**, *47*, 7592–7601.

(45) Cheong, P. H. Y.; Morganelli, P.; Luzung, M. R.; Houk, K. N.; Toste, F. D. *J. Am. Chem. Soc.* **2008**, *130*, 4517–4526.

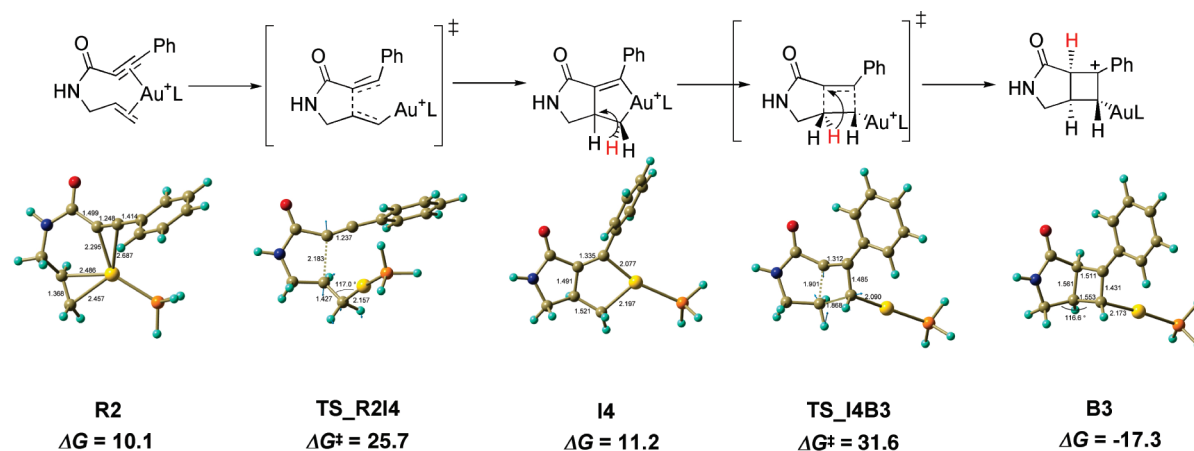


FIGURE 7. Reaction diagram of transformations from **R2** to the cyclobutene (**B3**) via metallacycle intermediate (**I4**). Geometries of stationary points are optimized structures via DFT at the B3LYP/6-31G(d) and LANL2DZ levels. ZPE corrected free energies are given in kcal/mol. Arrows (sky blue) in the transition state geometries indicate displacement vectors of vibrational mode possessing an imaginary frequency.

concerted (Figure 7). At this point, the phosphinegold(I) moiety is attached only to the terminal alkene with a Au—C(1) bond length of 2.157 Å. The Au—C(1)—C(2) angle is obtuse (117.0°) with the phosphinegold(I) moiety being positioned outward from the potential metallacycle plane. Displacement vectors of this transition state display major fluctuation between C(2) and C(6). Therefore, it appears that Au—C(7) bond formation to complete the metallacycle might occur after the C(2)—C(6) bond is formed.

The free energy of **R2** and **I4** is 10.1 and 9.4 kcal/mol higher than those of **R1** and **I3**, respectively. Likewise, the transition state **TS_R2I4** resides at 25.7 kcal/mol, which is 10.5 kcal/mol higher than that of **TS_R1I3**; this step is obviously disadvantageous relative to the **R1_I3** pathway.

It was necessary to suppose a third type of cyclobutene product that is different from **B1** or **B2** in terms of positions of phosphinegold(I) moiety and protons. If a C(1)—C(7) bond is formed from **I4**, the phosphinegold(I) moiety can be destined toward either C(7) or C(1). When we considered the former assumption, the resulting structure optimized by the DFT calculation was **B2**. **B3** was the optimized structure based on the assumption for the latter. It is important to note that a sequential repositioning of protons was prerequisite to adopt **B3** as a product as shown in Figure 7. **B3** has a similar free energy level with **B2**. The activation free energy from **I4** to **B3** was, however, prohibitively high ($\Delta G^\ddagger = 31.6$ kcal/mol) probably due to the proton movements. We also located the transition state that connects **I4** and **B2** (not shown). However, its activation free energy was 30.8 kcal/mol ($\Delta G^\ddagger = 46.0$ kcal/mol), which is even higher than that of **TS_I4B3**. From this result, the pathway through **I4** is obviously unfavorable. Figure 8 displays an overall free energy profile of cyclobutene formation of the amide-tethered 1,6-enyne system.

Comparison of the Effects of Carbonyl Group (C(5)) vs. Phenyl Group (C(7)). Virtually all examples of the cyclobutene formation by the transition metal-catalyzed cycloisomerization reaction of 1,6-enynes feature an aryl group at the terminal alkyne position.^{14,17} However, as we previously reported,³⁶ compound **3** gave rise to a bicyclo[4.1.0]hept-4-ene derivative **4** (eq 2) demonstrating that a mere introduc-

tion of an aryl group at the terminal alkyne position cannot drive the reaction to the cyclobutene product. However, it is somewhat hasty to conclude that the formation of cyclobutene product is solely due to the effect of the keto carbonyl group at the C(5) position. Hence, we performed DFT calculations for both no-carbonyl (Figure 9) and no-phenyl (Figure 10) systems to interrogate the relative effect of the keto carbonyl and the terminal aryl group on the reactivity of gold(I)-catalyzed cycloisomerization reaction.

In the system without keto carbonyl (Figure 9), the 6-*endo*-cyclization via **TS_NRI3** has the lowest free energy barrier ($\Delta G^\ddagger = 11.4$ kcal/mol). The free energy barriers for 5-*exo*-cyclizations were 15.4 kcal/mol (**TS_NRI1**) and 25.1 kcal/mol (**TS_NRI2**). This result suggests that a careful control of the reaction under mild conditions might lead to the formation of **NI3** exclusively although **TS_NRI3** lies only 4 kcal/mol lower than **TS_NRI1**. Interestingly, **NI3** ($\Delta G = -5.8$ kcal/mol) was similarly stable with **NI1** ($\Delta G = -3.4$ kcal/mol) or **NI2** ($\Delta G = -6.3$ kcal/mol). This pattern clearly differs from that of the amide-tethered analogue in which **I3** was mostly destabilized. Consequently, the activation free energy from **NI3** to **NB2** becomes as high as 15.2 kcal/mol even though the free energy of **TS_NI3B2** ($\Delta G^\ddagger = 9.4$ kcal/mol) is in a similar level with that of **TS_I3B2** ($\Delta G^\ddagger = 8.2$ kcal/mol). Note that the magnitudes of the activation free energies for both the forward and the reverse reactions from **NI3** are higher than that for the first step (**NR_NI3**), which drives the reaction entrapped at the **NI3** stage.³⁶

For the system without a phenyl group at the terminal alkyne position (Figure 10), calculation results were significantly different from those discussed above. First of all, the 5-*exo*-*anti*-cyclization via **TS_PRI1** has the lowest activation barrier from **PRI1** to cyclopropyl metal carbene intermediates. The free energy barrier of this state ($\Delta G^\ddagger = 6.6$ kcal/mol) is ca. 5 and 7 kcal/mol smaller than those of **TS_PRI3** ($\Delta G^\ddagger = 11.3$ kcal/mol) and **TS_PRI2** ($\Delta G^\ddagger = 13.3$ kcal/mol), respectively; the first step of the reaction is thus most likely toward **P1I** and the possibility of its being toward **I2** or **I3** is low.

The 5-*exo*-*anti* product **P1I** could evolve to either cyclobutene (**PB1**) via **TS_P1IB1** or 1,3-diene (**PD1**) via **TS_I1D1**. Whereas the process toward **PD1** is highly exothermic

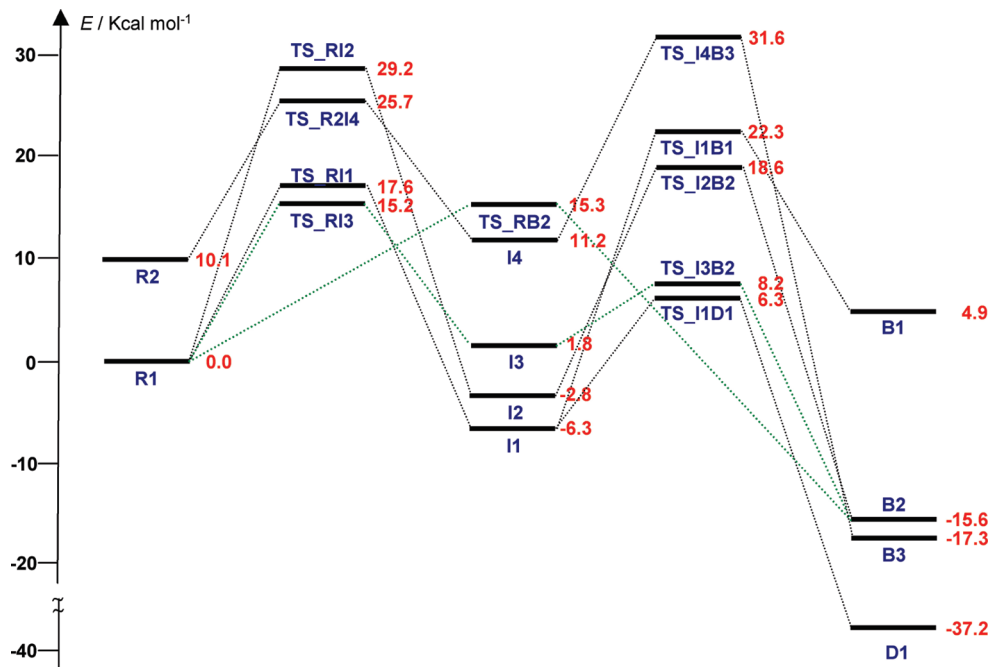


FIGURE 8. Free energy reaction profile of Au(I)-catalyzed cycloisomerization reactions of amide-tethered 7-phenyl-1,6-ene. Numbers in red denote free energies in kcal/mol. Green dotted lines signify most probable reaction pathways. For details of structures of all compounds listed in this diagram, see the SI.

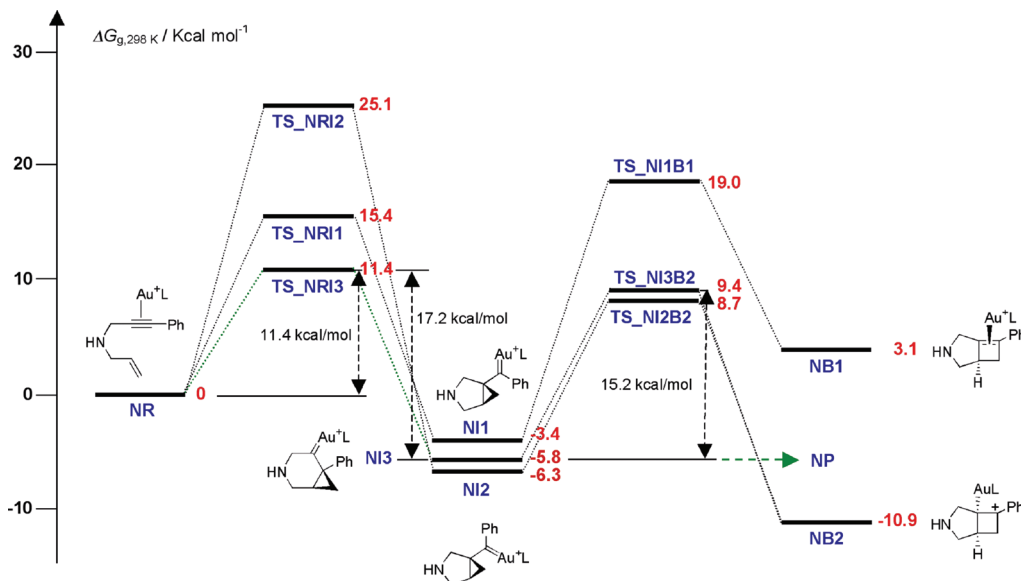


FIGURE 9. Free energy reaction profile of Au(I)-catalyzed cycloisomerization reactions of *N*-tethered 7-phenyl-1,6-ene. Numbers in red denote free energies in kcal/mol. Green dotted lines signify most probable reaction pathway. For details of structures of all compounds listed in this diagram, see the SI.

($\Delta G_{rxn} = 37.9$ kcal/mol), the **PI1_PB1** process is 9.5 kcal/mol uphill. Moreover, the activation free energy of the **PI1_PB1** process is 16.7 kcal/mol while that for the **PI1_PD1** process is only 2.1 kcal/mol. Thus the evolution from **PI1** is most likely to the 1,3-diene product.

Unlike the system possessing both the keto carbonyl and phenyl groups at C(5) and C(7), respectively, the 5-*exo-syn* product **PI2** gave rise to the formation of both cyclobutene (**PB2**) via **TS_PI2B2** or 1,3-diene (**PD2**) via **TS_I2D2**. The activation free energies for both processes are similar to each

other; they are 9.5 and 7.4 kcal/mol for **TS_PI2B2** or **TS_I2D2**, respectively. However, these values are still much higher than that of the **PI1_PD1** process. Thus the process involving the **I2** intermediate could not affect the overall reaction pathway. Likewise, the reaction pathway involving **I3** did not alter the destination of the reaction as shown in Figure 10. These results clearly show that the selective formation of a cyclobutene by the gold(I)-catalyzed cycloisomerization reaction of amide tethered 1,6-ene systems can be ascribed to the interplay of both the keto

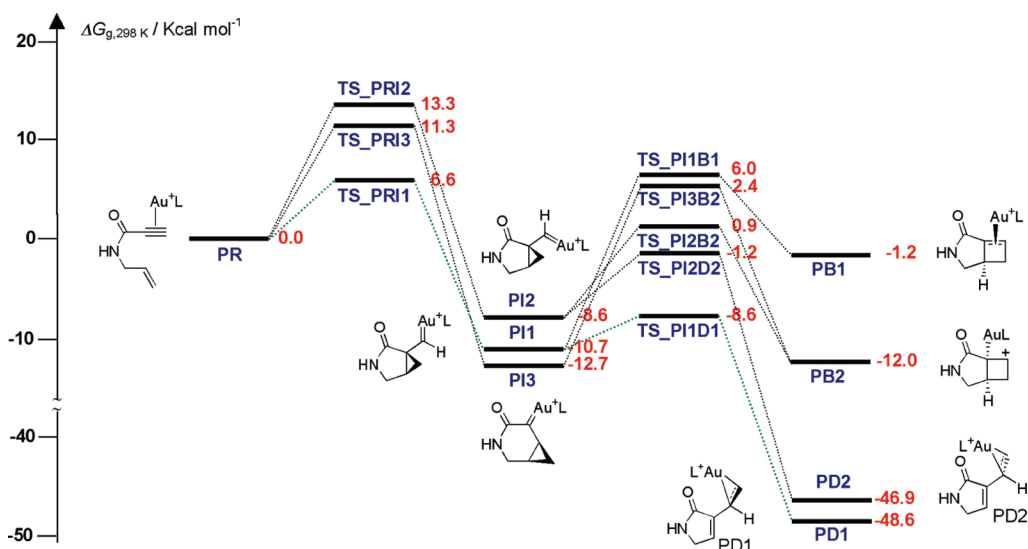


FIGURE 10. Free energy reaction profile of Au(I)-catalyzed cycloisomerization reactions of amide-tethered 1,6-ene. Numbers in red denote free energies in kcal/mol. Green dotted lines signify the most probable reaction pathway. For details of structures of all compounds listed in this diagram, see the SI.

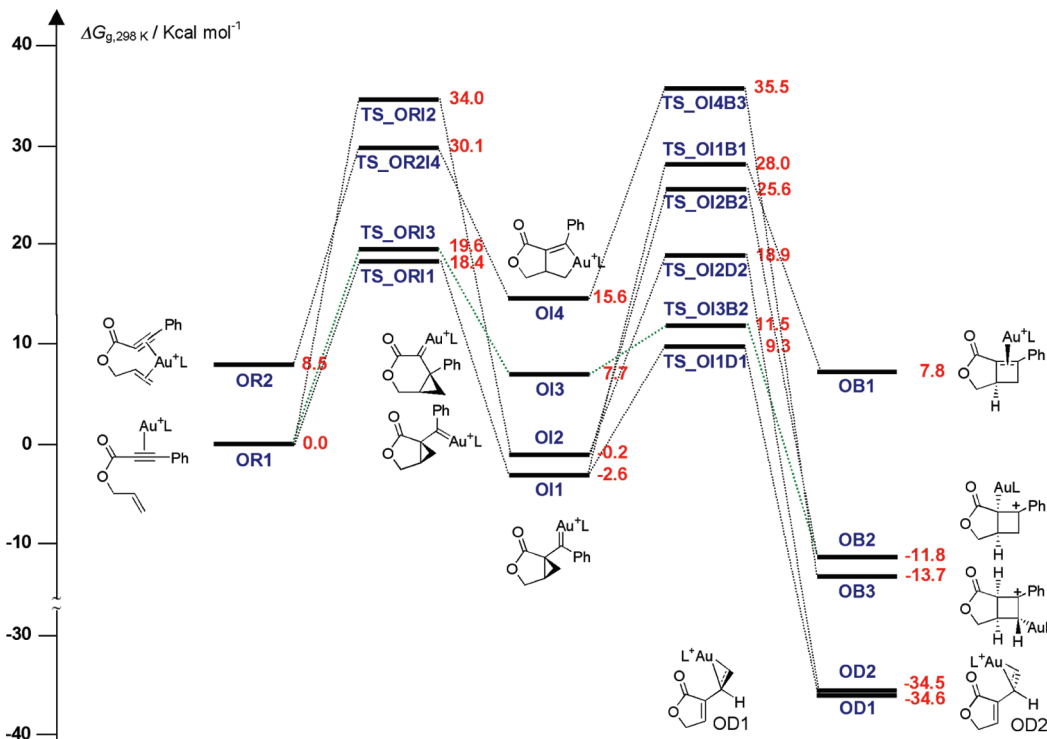


FIGURE 11. Free energy reaction profile of Au(I)-catalyzed cycloisomerization reactions of ester-tethered 7-phenyl-1,6-ene. Numbers in red denote free energies in kcal/mol. Green dotted lines signify the most probable reaction pathway. For details of structures of all compounds listed in this diagram, see the SI.

carbonyl group and the aryl substituent at C(5) and C(7) positions, respectively.

Mechanism of the Ester-Tethered System. We also investigated the ester-tethered 1,6-ene system. The overall feature of the reaction pathway obtained from the calculation is similar to that for the amide-tethered one (Figure 11). However, a number of points deserve comments. First, the free energy barrier from the reactant state (**OR**) to the 6-*endo*-cyclization product (**OI3**) was slightly higher

($\Delta G^\ddagger = 19.6 \text{ kcal/mol}$) than that to the 5-*exo-anti* product (**OI1**, $\Delta G^\ddagger = 18.4 \text{ kcal/mol}$) in this case. Thus the first step of the reaction cannot distinguish the 5-*exo-anti* and the 6-*endo* processes clearly. The differentiation between these two processes is made only in the second step.

OI1 can evolve either to **D1** or **B1** with the former being preferred. The activation free energy for the **OI1_OD1** process is 11.9 kcal/mol while that for the **OI1_OB1** process is 30.6 kcal/mol. On the other hand, **OI3** can be easily

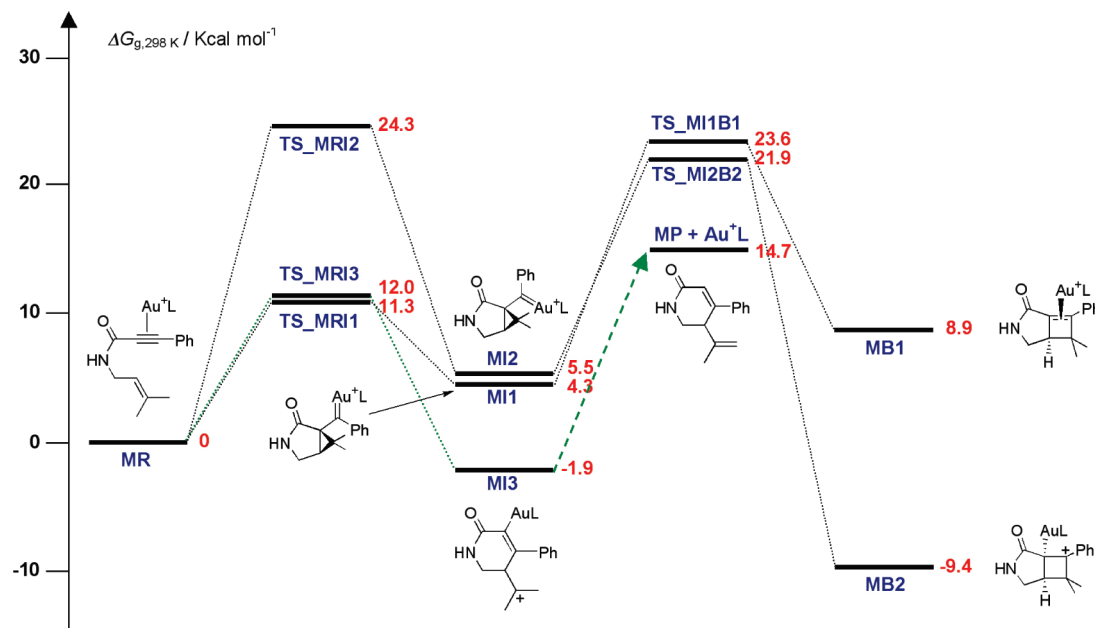


FIGURE 12. Free energy reaction profile of Au(I)-catalyzed cycloisomerization reactions of amide-tethered 1,1-dimethyl-7-phenyl-1,6-ene. Numbers in red denote free energies in kcal/mol. Green dotted lines signify the most probable reaction pathway. For details of structures of all compounds listed in this diagram, see the SI.

transformed into **OB2** with only 3.8 kcal/mol of activation free energy. Therefore, the formation of cyclobutene is still advantageous to that of 1,3-diene in the ester-tethered system.

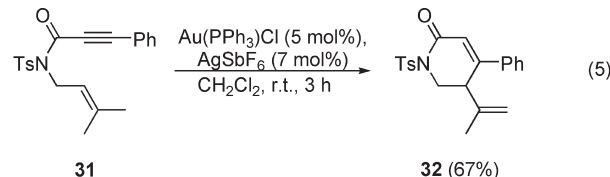
Second, the magnitude of the activation free energy of the **OR_OI3** step ($\Delta G^\ddagger = 19.6$ kcal/mol) is ca. 4 kcal/mol larger than that of the **R1_I 3** step in the amide-tethered system ($\Delta G^\ddagger = 15.2$ kcal/mol). Since this step is rate-determining, this result implies that the ester-tethered system requires more time to complete the reaction than the amide-tethered one. Actually, the ester-tethered system requires 12 h of average reaction time while the amide-tethered one requires only half an hour.

Third, the reaction pathway bifurcation was not observed in this case. **TS_ORI3** could not connect **R1** to **OB2**. This point combined with the fact that the lowest barrier of the first step is not **TS_ORI3** but **TS_ORI1** drives the situation where the formation of **OI1** is unavoidable, which gives rise to the formation of 1,3-diene as a minor product in some cases (Table 1, entries 4 and 5).

Mechanism of the 1,1-Dimethyl-1,6-ene Systems. When both protons at the terminal alkenyl position were substituted with methyl groups, the desired cyclobutene was not synthesized. Instead, the 5,6-dihydropyridin-2(1H)-one derivative was obtained (eq 5). The identity of the product was verified by X-ray crystallography (see the SI). This result is in sharp contrast to those observed in allylpropargylmalonate systems in which cationic gold(I) led to the formation of 2,3,9,9a-tetrahydro-1*H*-cyclopenta[*b*]naphthalenes by intramolecular [4+2] cycloadditions.^{14,17}

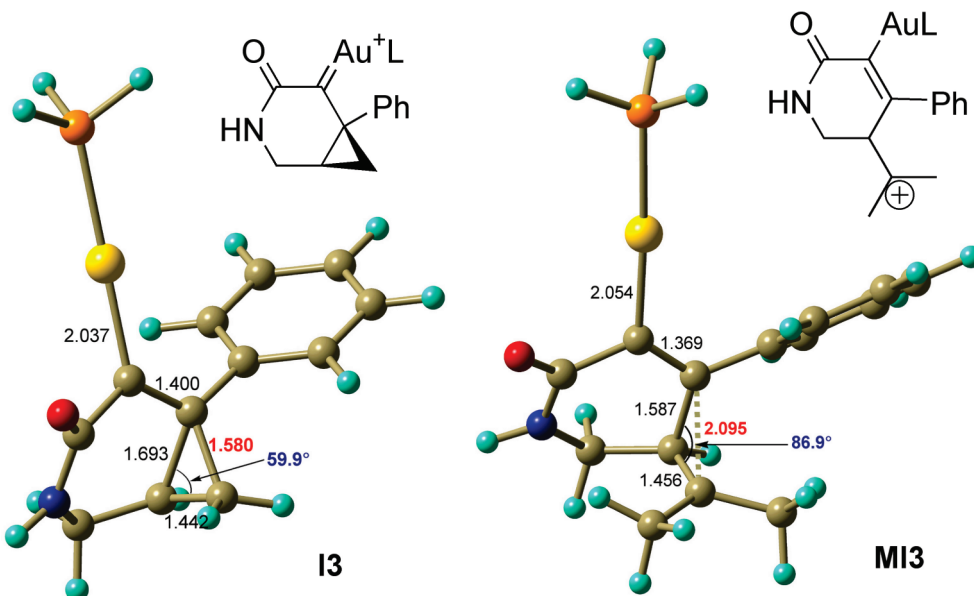
To investigate the background of this result, we performed DFT calculations. Figure 12 illustrates the whole profiles of reaction energetics. Both the 5-*exo*-anti- and the 6-*endo*-cyclizations have similar activation free energies (~12 kcal/mol). The activation free energy of the 5-*exo*-syn-cyclization is a factor of 2 larger than the other two (24.3 kcal/mol) and

thus we can safely exclude the pathway involving **MI2**. Since **TS_MRI1** and **TS_MRI3** are virtually isoenergetic, both the 5-*exo*- and the 6-*endo*-cyclizations have an equal opportunity. However, it is important to note that the **MR_MI1** process is endothermic by 4.3 kcal/mol while the **MR_MI3** process is slightly exothermic ($\Delta G_{rxn} = -1.9$ kcal/mol).



The structure of **MI1** resembles its archetypal **I1** except that the C(1)–C(2) and the C(1)–C(6) bond distances of **MI1** are slightly longer than those of **I1** (see the SI for detailed structural information). Notable differences were observed in the structure of **MI3**. The comparison of two structures (**I3** and **MI3**) is depicted in Figure 13.

In **MI3**, the C(1)–C(7) distance was 2.095 Å indicating that there is no more bonding character between two carbon atoms. The C(1)–C(2)–C(7) angle (86.9°) of **MI3** also exhibits the breakdown of the cyclopropyl skeleton. As a result, the positive charge was built at the C(1) atom. The Mulliken charge at this position of **MI3** obtained by DFT calculation was 0.221 while that of **I3** was −0.288. Nevertheless, the free energy level of **MI3** ($\Delta G = -1.9$ kcal/mol) lies lower than those of **MI1** ($\Delta G = 4.3$ kcal/mol) or **MI2** ($\Delta G = 5.5$ kcal/mol). Considering the fact that **I3** has a higher free energy than **I1** or **I2**, this result was noteworthy. It is probably due to the stabilization of the positive charge by the two adjacent methyl groups. This structural variation gave rise to a completely different consequence. The transformation from **MI3** to the cyclobutene was no longer possible. In **TS_I3B2**, the C(1)–C(7) bond plays a pinning

**FIGURE 13.** Geometry comparison of **I3** and **MI3**.

role during the bond-forming fluctuation between C(2) and C(6). However, this type of fluctuation cannot be accomplished in **MI3** because the C(1)–C(7) bond is no longer available. As expected, the transition state between **MI3** and **MB2** could not be located in spite of the elaborate computational search. On the other hand, **MI1** could evolve to cyclobutene **MB1** with 19.3 kcal/mol of activation barrier. Note that the formation of 5,6-dihydropyridin-2(1*H*)-one by demetalation requires only 16.6 kcal/mol of energy. Hence, the gold(I)-catalyzed cycloisomerization reaction of amide-tethered 1,1-dimethyl-1,6-enyne substrate resulted in the formation of 5,6-dihydropyridin-2(1*H*)-one.

Conclusion

The Au(I)-catalyzed cycloisomerization of amide- or ester-tethered 1,6-enynes gave bicyclo[3.2.0]hept-6-en-2-ones in reasonable to high yields. A subtle change in the substrate completely alters the reaction pathway. This reaction can be complementary to the platinum- or gold(I)-catalyzed formation of cyclobutenes from enynes with a carbon chain. Calculations carried out on the Au(I)-catalyzed formation of cyclobutenes also support this experimental observation. Further work on amide- or ester-tethered enynes in other transition metal-catalyzed processes is underway in our laboratories.

Experimental Section

General Procedure for the Au(I)-Catalyzed Cycloisomerization Reaction of Amide- or Ester-Tethered 1,6-Enynes. To a flame-dried 15-mL Schlenk flask capped with a rubber septum was injected via a syringe 5 mL of dichloromethane under N₂ flow. Au(PPh₃)Cl (25 mg, 10 mol %) and AgSbF₆ (24 mg, 14 mol %) were added sequentially. The solution was stirred for 10 min. A 1,6-enyne bearing a keto carbonyl (0.5 mmol) was put into the flask under N₂ flow. The reaction was monitored by thin-layer chromatography. After the reactant disappeared, the solvent was removed under reduced pressures. Flash chromatography on a silica gel eluting with hexane and ethyl acetate (v/v, 10:1) gave the product.

7-Phenyl-3-tosyl-3-aza-bicyclo[3.2.0]hept-6-en-2-one (2): ¹H NMR (CDCl₃, 300 MHz) δ 2.39 (s, 3 H), 3.33 (dd, *J* = 3.9, 8.0 Hz, 1 H), 3.86 (dd, *J* = 8.0, 10.5 Hz, 1 H), 3.86 (m, 1 H), 4.03 (d, *J* = 10.5 Hz, 1 H), 6.43 (s, 1 H), 7.27 (d, *J* = 8.3 Hz, 2 H), 7.31 (m, 3 H), 7.46 (m, 2 H), 7.90 (d, *J* = 8.3 Hz, 2 H); ¹³C NMR (CDCl₃, 75 MHz) δ 21.6, 32.9, 48.5, 49.4, 125.2, 128.1, 128.4, 128.9, 129.2, 129.5, 131.7, 134.8, 145.0, 148.4, 171.9; IR ν_{CO} (CHCl₃) 1723.2 cm⁻¹; HRMS (EI) calcd for C₁₉H₁₇N₁O₃S₁(M⁺) 339.0929, found 339.0929.

6-Methyl-7-phenyl-3-oxa-bicyclo[3.2.0]hept-6-en-2-one (6): ¹H NMR (CDCl₃, 500 MHz) δ 2.10 (t, *J* = 1.5 Hz, 3 H), 3.45 (m, 1 H), 3.83 (dq, *J* = 1.8, 3.6 Hz, 1 H), 4.34 (m, 2 H), 7.27 (m, 1 H), 7.37 (m, 2 H), 7.53 (m, 2 H); ¹³C NMR (CDCl₃, 125 MHz) δ 14.1, 40.7, 43.6, 67.5, 126.2, 127.9, 128.6, 133.2, 140.2, 141.1, 175.7; IR ν_{CO} (CHCl₃) 1748.8 cm⁻¹; HRMS (EI) calcd for C₁₃H₁₂O₂(M⁺) 200.0837, found 200.0834.

(E)-3-(1-Phenylprop-1-enyl)furan-2(5*H*)-one (7): ¹H NMR (CDCl₃, 500 MHz) δ 1.67 (d, *J* = 7.1 Hz, 3 H), 4.72 (m, 2 H), 6.67 (m, 1 H), 7.16 (m, 2 H), 7.25 (q, *J* = 7.1 Hz, 1 H), 7.34 (m, 1 H), 7.41 (m, 2 H); ¹³C NMR (CDCl₃, 125 MHz) δ 15.3, 68.9, 127.3, 128.5, 129.2, 129.7, 132.1, 132.6, 138.1, 144.1, 172.0; IR ν_{CO} (CHCl₃) 1748.0 cm⁻¹; HRMS (EI) calcd for C₁₃H₁₂O₂(M⁺) 200.0837, found 200.0836.

Diethyl 2-(2-methylallyl)-2-(3-phenylpropioloyl)malonate (8): ¹H NMR (CDCl₃, 500 MHz) δ 1.28 (t, *J* = 7.1 Hz, 6 H), 1.76 (s, 3 H), 3.09 (s, 2 H), 4.28 (q, *J* = 7.1 Hz, 4 H), 4.81 (s, 1 H), 4.87 (s, 1 H), 7.39 (m, 2 H), 7.48 (m, 1 H), 7.57 (m, 2 H); ¹³C NMR (CDCl₃, 125 MHz) δ 13.9, 23.4, 40.2, 62.2, 71.3, 86.5, 94.5, 115.7, 119.6, 128.7, 131.1, 133.1, 140.3, 166.2, 178.6; IR ν_{CO} (CHCl₃) 1672.0, 1737.6 cm⁻¹; HRMS (EI) calcd for C₂₀H₂₂O₅(M⁺) 342.1467, found 342.1470.

Diethyl 4-methyl-2-oxo-3-(1-phenylvinyl)cyclopent-3-ene-1,1-dicarboxylate (9): ¹H NMR (CDCl₃, 500 MHz) δ 1.30 (t, *J* = 7.1 Hz, 6 H), 2.00 (s, 3 H), 3.28 (m, 2 H), 4.28 (q, *J* = 7.1 Hz, 4 H), 5.26 (d, *J* = 1.1 Hz, 1 H), 5.84 (d, *J* = 1.1 Hz, 1 H), 7.28 (m, 5 H); ¹³C NMR (CDCl₃, 125 MHz) δ 13.9, 18.1, 41.3, 62.4, 65.3, 118.2, 126.1, 127.8, 128.4, 138.6, 138.7, 138.8, 167.0, 171.6, 194.8; IR ν_{CO} (CHCl₃) 1636.8, 1718.4 cm⁻¹; HRMS (EI) calcd for C₂₀H₂₂O₅(M⁺) 342.1467, found 342.1466.

N-(2-Methylallyl)-3-phenyl-N-tosylpropiolamide (10): ¹H NMR (CDCl₃, 500 MHz) δ 1.81 (s, 3 H), 2.43 (s, 3 H), 4.63 (s, 2 H), 5.00 (s, 1 H), 5.02 (s, 1 H), 7.30 (d, *J* = 8.3 Hz, 2 H), 7.38 (m, 2 H), 7.46 (m, 1 H), 7.50 (m, 2 H), 7.93 (d, *J* = 8.3 Hz, 2 H);

¹³C NMR (CDCl₃, 125 MHz) δ 20.2, 21.6, 52.4, 81.5, 92.6, 112.9, 119.4, 128.7, 128.9, 129.3, 130.9, 132.7, 135.7, 139.8, 145.1, 152.9; IR ν_{CO} (CHCl₃) 1664.0 cm⁻¹; HRMS (EI) calcd for C₂₀H₁₉N₁O₃S₁ (M⁺) 353.1086, found 353.1089.

5-Methyl-7-phenyl-3-tosyl-3-aza-bicyclo[3.2.0]hept-6-en-2-one (11): ¹H NMR (CDCl₃, 500 MHz) δ 1.43 (s, 3 H), 2.40 (s, 3 H), 3.44 (s, 1 H), 3.59 (d, J = 10.5 Hz, 1 H), 4.06 (d, J = 10.5 Hz, 1 H), 6.47 (s, 1 H), 7.27 (d, J = 6.8 Hz, 2 H), 7.32 (m, 3 H), 7.46 (m, 2 H), 7.90 (d, J = 6.8 Hz, 2 H); ¹³C NMR (CDCl₃, 125 MHz) δ 21.6 (2 C), 40.1, 54.1, 54.9, 125.3, 128.1, 128.4, 128.8, 129.5, 131.8, 133.5, 134.9, 145.0, 146.2, 172.3; IR ν_{CO} (CHCl₃) 1726.4 cm⁻¹; HRMS (EI) calcd for C₂₀H₁₉N₁O₃S₁ (M⁺) 353.1086, found 353.1088.

N-(But-2-enyl)-3-phenyl-N-tosylpropiolamide (12): ¹H NMR (CDCl₃, 500 MHz) δ 1.73 (trans) (d, J = 6.3 Hz, 3 H), 1.8 (cis) (d, J = 6.9 Hz, 3 H), 2.41 (s, 3 H), 4.62 (trans) (d, J = 6.0 Hz, 2 H), 4.75 (cis) (d, J = 6.4 Hz, 2 H), 5.55 (cis) (m, 1 H), 5.62 (trans) (m, 1 H), 5.73 (cis) (m, 1 H), 5.86 (trans) (m, 1 H), 7.29 (d, J = 7.1 Hz, 2 H), 7.38 (m, 2 H), 7.46 (m, 1 H), 7.51 (m, 2 H), 7.89 (d, J = 7.1 Hz, 2 H); ¹³C NMR (CDCl₃, 125 MHz) δ 17.6, 21.5, 48.9, 81.6, 92.7, 119.4, 125.2, 128.6, 129.2, 129.3, 130.8, 130.9, 132.6, 136.0, 144.9, 152.5; IR ν_{CO} (CHCl₃) 1660.8 cm⁻¹; HRMS (EI) calcd for C₂₀H₁₉N₁O₃S₁ (M⁺) 353.1086, found 353.1089.

6-Methyl-7-phenyl-3-tosyl-3-aza-bicyclo[3.2.0]hept-6-en-2-one (13): ¹H NMR (CDCl₃, 500 MHz) δ 2.07 (s, 3 H), 2.40 (s, 3 H), 3.19 (dd, J = 3.9, 8.3 Hz, 1 H), 3.69 (m, 1 H), 3.77 (d, J = 8.3, 10.6 Hz, 1 H), 4.04 (d, J = 10.6 Hz, 1 H), 7.23 (m, 1 H), 7.27 (d, J = 8.0 Hz, 2 H), 7.31 (m, 2 H), 7.43 (m, 2 H), 7.89 (d, J = 8.3 Hz, 2 H); ¹³C NMR (CDCl₃, 125 MHz) δ 13.9, 21.6, 35.7, 46.5, 47.4, 126.3, 127.8, 128.1, 128.4, 129.5, 133.1, 135.0, 140.3, 140.8, 145.0, 172.5; IR ν_{CO} (CHCl₃) 1728.0 cm⁻¹; HRMS (EI) calcd for C₂₀H₁₉N₁O₃S₁ (M⁺) 353.1086, found 353.1089.

But-2-enyl 3-p-tolylpropiolate (14): ¹H NMR (CDCl₃, 500 MHz) δ 1.75 (d, J = 6.5 Hz, 3 H), 2.38 (s, 3 H), 4.65 (trans) (d, J = 6.7 Hz, 2 H), 4.80 (cis) (d, J = 7.0 Hz, 2 H), 5.62 (cis) (m, 1 H), 5.65 (trans) (m, 1 H), 5.79 (cis) (m, 1 H), 5.88 (trans) (m, 1 H), 7.17 (d, J = 8.0 Hz, 2 H), 7.47 (d, J = 8.0 Hz, 2 H); ¹³C NMR (CDCl₃, 125 MHz) δ 21.6, 21.7, 66.6, 80.2, 86.8, 116.5, 124.2, 129.3, 132.7, 133.0, 141.2, 154.0; IR ν_{CO} (CHCl₃) 1705.6 cm⁻¹; HRMS (EI) calcd for C₁₄H₁₄O₂ (M⁺) 214.0994, found 214.0995.

6-Methyl-7-p-tolyl-3-oxa-bicyclo[3.2.0]hept-6-en-2-one (15): ¹H NMR (CDCl₃, 500 MHz) δ 2.07 (t, J = 1.5 Hz, 3 H), 2.34 (s, 3 H), 3.43 (m, 1 H), 3.80 (dq, J = 1.7, 3.6 Hz, 1 H), 4.33 (m, 2 H), 7.17 (d, J = 8.2 Hz, 2 H), 7.42 (d, J = 8.2 Hz, 2 H); ¹³C NMR (CDCl₃, 125 MHz) δ 14.0, 21.3, 40.6, 43.5, 67.5, 126.1, 129.2, 130.4, 137.9, 139.8, 140.1, 175.8; IR ν_{CO} (CHCl₃) 1746.4 cm⁻¹; HRMS (EI) calcd for C₁₄H₁₄O₂ (M⁺) 214.0994, found 214.0996.

(E)-3-(1-p-Tolylprop-1-enyl)furan-2(5H)-one (16): ¹H NMR (CDCl₃, 500 MHz) δ 1.67 (d, J = 7.0 Hz, 3 H), 2.39 (s, 3 H), 4.71 (m, 1 H), 4.72 (m, 1 H), 6.69 (m, 1 H), 7.04 (d, J = 7.9 Hz, 2 H), 7.21 (d, J = 7.9 Hz, 2 H), 7.22 (q, J = 7.0 Hz, 1 H); ¹³C NMR (CDCl₃, 125 MHz) δ 15.3, 21.2, 68.9, 129.1, 129.2, 129.6, 132.3, 132.5, 135.0, 137.0, 144.1, 172.0; IR ν_{CO} (CHCl₃) 1733.6 cm⁻¹; HRMS (EI) calcd for C₁₄H₁₄O₂ (M⁺) 214.0994, found 214.0998.

5-Methyl-7-phenyl-3-oxa-bicyclo[3.2.0]hept-6-en-2-one (18): ¹H NMR (CDCl₃, 500 MHz) δ 1.49 (s, 3 H), 3.55 (s, 1 H), 4.10 (d, J = 9.6 Hz, 1 H), 4.34 (d, J = 9.6 Hz, 1 H), 6.52 (s, 1 H), 7.30 (m, 1 H), 7.36 (m, 2 H), 7.53 (m, 2 H); ¹³C NMR (CDCl₃, 125 MHz) δ 20.2, 44.9, 51.3, 74.6, 125.2, 128.5, 128.9, 131.9, 133.6, 146.1, 175.4; IR ν_{CO} (CHCl₃) 1766.4 cm⁻¹; HRMS (EI) calcd for C₁₃H₁₂O₂ (M⁺) 200.0837, found 200.0839.

2-Methylallyl 3-p-tolylpropiolate (19): ¹H NMR (CDCl₃, 500 MHz) δ 1.81 (s, 3 H), 2.36 (s, 3 H), 4.64 (s, 2 H), 4.99 (s, 1 H), 5.06 (s, 1 H), 7.17 (d, J = 7.9 Hz, 2 H), 7.47 (d, J = 7.9 Hz, 2 H); ¹³C NMR (CDCl₃, 125 MHz) δ 19.3, 21.5, 68.9, 80.1, 86.9, 113.8, 116.3, 129.2, 132.8, 139.0, 141.2, 153.7; IR ν_{CO} (CHCl₃) 1705.6

cm⁻¹; HRMS (EI) calcd for C₁₄H₁₄O₂ (M⁺) 214.0994, found 214.0996.

5-Methyl-7-p-tolyl-3-oxa-bicyclo[3.2.0]hept-6-en-2-one (20): ¹H NMR (CDCl₃, 500 MHz) δ 1.48 (s, 3 H), 2.34 (s, 3 H), 3.52 (s, 1 H), 4.09 (d, J = 9.6 Hz, 1 H), 4.33 (d, J = 9.6 Hz, 1 H), 6.45 (s, 1 H), 7.16 (d, J = 7.9 Hz, 2 H), 7.42 (d, J = 7.9 Hz, 2 H); ¹³C NMR (CDCl₃, 125 MHz) δ 20.3, 21.4, 44.8, 51.2, 74.7, 125.1, 129.2 (2 C), 132.4, 139.0, 146.0, 175.6; IR ν_{CO} (CHCl₃) 1747.2 cm⁻¹; HRMS (EI) calcd for C₁₄H₁₄O₂ (M⁺) 214.0994, found 214.0993.

(E)-2-Methylbut-2-enyl 3-phenylpropiolate (21): ¹H NMR (CDCl₃, 500 MHz) δ 1.66 (dq, J = 1.0, 10 Hz, 3 H), 1.72 (q, J = 1.0 Hz, 3 H), 4.62 (s, 2 H), 5.64 (m, 1 H), 7.37 (m, 2 H), 7.45 (m, 1 H), 7.59 (m, 2 H); ¹³C NMR (CDCl₃, 125 MHz) δ 13.3, 13.7, 71.9, 80.6, 86.2, 119.7, 125.6, 128.5, 139.9, 130.6, 133.0, 154.1; IR ν_{CO} (CHCl₃) 1700.8 cm⁻¹; HRMS (EI) calcd for C₁₄H₁₄O₂ (M⁺) 214.0994, found 214.0991.

5,6-Dimethyl-7-phenyl-3-oxa-bicyclo[3.2.0]hept-6-en-2-one (22): ¹H NMR (CDCl₃, 500 MHz) δ 1.44 (s, 3 H), 2.04 (d, J = 1.8 Hz, 3 H), 3.45 (q, J = 1.8 Hz, 1 H), 4.00 (d, J = 9.7 Hz, 1 H), 4.33 (d, J = 9.7 Hz, 1 H), 7.27 (m, 1 H), 7.37 (m, 2 H), 7.53 (m, 2 H); ¹³C NMR (CDCl₃, 125 MHz) δ 11.5, 18.3, 46.2, 49.9, 72.4, 126.2, 127.8, 128.5, 133.2, 137.9, 144.5, 176.0; IR ν_{CO} (CHCl₃) 1752.8 cm⁻¹; HRMS (EI) calcd for C₁₄H₁₄O₂ (M⁺) 214.0994, found 214.0992.

(E)-2-Methylbut-2-enyl 3-p-tolylpropiolate (23): ¹H NMR (CDCl₃, 300 MHz) δ 1.66 (d, J = 6.6 Hz, 3 H), 1.71 (s, 3 H), 2.38 (s, 3 H), 4.61 (s, 2 H), 5.63 (q, J = 6.6 Hz, 2 H), 7.17 (d, J = 8.1 Hz, 2 H), 7.48 (d, J = 8.1 Hz, 2 H); ¹³C NMR (CDCl₃, 75 MHz) δ 13.3, 13.7, 21.7, 71.8, 80.3, 86.7, 116.6, 125.5, 129.3, 130.0, 133.0, 141.2, 154.2; IR ν_{CO} (CHCl₃) 1696.8 cm⁻¹; HRMS (EI) calcd for C₁₅H₁₆O₂ (M⁺) 228.1150, found 228.1151.

5,6-Dimethyl-7-p-tolyl-3-oxa-bicyclo[3.2.0]hept-6-en-2-one (24): ¹H NMR (CDCl₃, 500 MHz) δ 1.42 (s, 3 H), 2.01 (d, J = 1.8 Hz, 3 H), 2.34 (s, 3 H), 3.41 (q, J = 1.8 Hz, 1 H), 3.99 (d, J = 9.6 Hz, 1 H), 4.31 (d, J = 9.6 Hz, 1 H), 7.17 (d, J = 8.0 Hz, 2 H), 7.41 (d, J = 8.0 Hz, 2 H); ¹³C NMR (CDCl₃, 125 MHz) δ 11.5, 18.4, 21.3, 46.2, 49.9, 72.5, 126.1, 129.2, 130.5, 137.8, 137.9, 143.2, 176.2; IR ν_{CO} (CHCl₃) 1748.8 cm⁻¹; HRMS (EI) calcd for C₁₅H₁₆O₂ (M⁺) 228.1150, found 228.1149.

N-Cyclohexenylmethyl-3-phenyl-N-tosylpropiolamide (25): ¹H NMR (CDCl₃, 500 MHz) δ 1.58 (m, 4 H), 1.93 (m, 2 H), 2.06 (m, 2 H), 2.43 (s, 3 H), 4.61 (s, 2 H), 5.77 (m, 1 H), 7.30 (d, J = 8.2 Hz, 2 H), 7.38 (m, 2 H), 7.46 (m, 1 H), 7.51 (m, 2 H), 7.91 (d, J = 8.2 Hz, 2 H); ¹³C NMR (CDCl₃, 125 MHz) δ 21.7, 22.1, 22.4, 25.0, 26.1, 52.9, 81.7, 92.7, 119.5, 125.7, 128.7, 128.9, 129.2, 130.9, 132.3, 132.7, 135.9, 144.9, 153.1; IR ν_{CO} (CHCl₃) 1660.8 cm⁻¹; HRMS (FAB) calcd for C₂₃H₂₄N₁O₃S₁ ([M + H]⁺) 394.1477, found 394.1480.

2-Tosyl-4-phenylbenzo[1,4]cyclobuta[1,2-c]pyrrole-3(3aH)-one, pentahydro (26): ¹H NMR (CDCl₃, 500 MHz) δ 1.35 (m, 2 H), 1.67 (m, 1 H), 1.77 (m, 1 H), 1.98 (m, 1 H), 2.03 (m, 1 H), 2.30 (m, 1 H), 2.40 (s, 3 H), 2.81 (m, 1 H), 3.43 (d, J = 2.3 Hz, 1 H), 3.52 (d, J = 10.2 Hz, 1 H), 4.17 (d, J = 10.2 Hz, 1 H), 7.22 (m, 1 H), 7.28 (d, J = 8.2 Hz, 2 H), 7.31 (m, 2 H), 7.41 (m, 2 H), 7.90 (d, J = 8.2 Hz, 2 H); ¹³C NMR (CDCl₃, 125 MHz) δ 21.7, 22.5, 24.6, 26.2, 35.4, 39.9, 52.2, 53.9, 126.2, 127.7, 128.1, 128.4, 129.5, 133.2, 135.0, 135.4, 144.9, 147.4, 172.6; IR ν_{CO} (CHCl₃) 1716.0 cm⁻¹; HRMS (FAB) calcd for C₂₃H₂₄N₁O₃S₁ ([M + H]⁺) 394.1477, found 394.1478.

Cyclohexenylmethyl-3-phenylpropioliate (27): ¹H NMR (CDCl₃, 500 MHz) δ 1.61 (m, 2 H), 1.69 (m, 2 H), 2.07 (m, 4 H), 4.61 (s, 2 H), 5.84 (m, 1 H), 7.38 (m, 2 H), 7.46 (m, 1 H), 7.60 (m, 2 H); ¹³C NMR (CDCl₃, 125 MHz) δ 22.0, 22.3, 25.0, 25.9, 70.5, 80.6, 86.2, 119.7, 127.8, 128.5, 130.6, 132.1, 133.0, 154.1; IR ν_{CO} (CHCl₃) 1700.8 cm⁻¹; HRMS (EI) calcd for C₁₆H₁₆O₂ (M⁺) 240.1150, found 240.1148.

1*H*-4-Phenylbenzo[1,4]cyclobuta[1,2-*c*]furan-3(3*aH*)-one, pentahydro (28): ^1H NMR (CDCl_3 , 500 MHz) δ 1.27 (m, 1 H), 1.40 (m, 1 H), 1.81 (m, 2 H), 1.99 (m, 1 H), 2.16 (m, 1 H), 2.31 (m, 1 H), 2.86 (m, 1 H), 3.57 (d, $J = 2.3$ Hz, 1 H), 4.11 (d, $J = 9.4$ Hz, 1 H), 4.47 (d, $J = 9.4$ Hz, 1 H), 7.26 (m, 1 H), 7.36 (m, 2 H), 7.50 (m, 2 H); ^{13}C NMR (CDCl_3 , 125 MHz) δ 22.9, 24.8, 26.0, 34.0, 44.6, 50.0, 72.9, 126.1, 127.8, 128.6, 133.3, 135.2, 147.4, 175.7; IR ν_{CO} (CHCl_3) 1753.6 cm^{-1} ; HRMS (EI) calcd for $\text{C}_{16}\text{H}_{16}\text{O}_2$ (M^+) 240.1150, found 240.1148.

Cyclohexenylmethyl 3-p-tolylpropiolate (29): ^1H NMR (CDCl_3 , 300 MHz) δ 1.64 (m, 4 H), 2.05 (m, 4 H), 2.38 (s, 3 H), 4.59 (s, 2 H), 5.82 (m, 1 H), 7.17 (d, $J = 8.0$ Hz, 2 H), 7.48 (d, $J = 8.0$ Hz, 2 H); ^{13}C NMR (CDCl_3 , 75 MHz) δ 21.7, 22.0, 22.3, 25.1, 25.9, 70.4, 80.3, 86.8, 116.6, 127.7, 129.3, 132.2, 133.0, 141.2, 154.2; IR ν_{CO} (CHCl_3) 1692.8 cm^{-1} ; HRMS (EI) calcd for $\text{C}_{17}\text{H}_{18}\text{O}_2$ (M^+) 254.1307, found 254.1306.

1*H*-4-(4-Methylphenyl)benzo[1,4]cyclobuta[1,2-*c*]furan-3(3*aH*)-one, pentahydro (30): ^1H NMR (CDCl_3 , 500 MHz) δ 1.24 (m, 1 H), 1.38 (m, 1 H), 1.79 (m, 2 H), 1.96 (m, 1 H), 2.13 (m, 1 H), 2.28 (m, 1 H), 2.34 (s, 3 H), 2.82 (m, 1 H), 3.53 (d, $J = 2.3$ Hz, 1 H), 4.09 (d, $J = 9.4$ Hz, 1 H), 4.45 (d, $J = 9.4$ Hz, 1 H), 7.15 (d, $J = 8.0$ Hz, 2 H), 7.39 (d, $J = 8.0$ Hz, 2 H); ^{13}C NMR (CDCl_3 , 125 MHz) δ 21.3, 22.9, 24.7, 26.0, 34.0, 44.5, 50.0, 73.0, 126.0, 129.2, 130.5, 135.1, 137.7, 146.1, 175.8; IR ν_{CO} (CHCl_3) 1745.6 cm^{-1} ; HRMS (EI) calcd for $\text{C}_{17}\text{H}_{18}\text{O}_2$ (M^+) 254.1307, found 254.1303.

N-(3-Methylbut-2-enyl)-3-phenyl-N-tosylpropiolamide (31): ^1H NMR (CDCl_3 , 500 MHz) δ 1.76 (s, 3 H), 1.81 (s, 3 H), 2.42 (s, 3 H), 4.69 (d, $J = 6.8$ Hz, 2 H), 5.29 (m, 1 H), 7.29 (d, $J = 8.4$ Hz, 2 H), 7.38 (m, 2 H), 7.46 (m, 1 H), 7.52 (m, 2 H), 7.88 (d, $J = 8.4$ Hz, 2 H); ^{13}C NMR (CDCl_3 , 125 MHz) δ 18.2, 21.7, 25.7, 45.6, 81.7, 93.0, 119.4, 128.5, 128.6, 128.7, 129.3, 129.7, 130.9, 132.7, 137.3, 144.9, 152.7; IR ν_{CO} (CHCl_3) 1664.0 cm^{-1} ; HRMS (EI) calcd for $\text{C}_{21}\text{H}_{21}\text{N}_1\text{O}_3\text{S}_1$ (M^+) 367.1242, found 367.1241.

4-Phenyl-5-(prop-1-en-2-yl)-1-tosyl-5,6-dihydropyridin-2(1*H*)-one (32): ^1H NMR (CDCl_3 , 500 MHz) δ 1.99 (s, 3 H), 2.42 (s, 3 H), 3.50 (m, 1 H), 3.87 (dd, $J = 4.2, 12.8$ Hz, 1 H), 4.66 (dd, $J = 2.1, 12.8$ Hz, 1 H), 4.73 (s, 1 H), 4.99 (s, 1 H), 6.32 (s, 1 H), 7.30 (d, $J = 8.2$ Hz, 2 H), 7.38 (m, 3 H), 7.45 (m, 2 H), 7.91 (d, $J = 8.4$ Hz, 2 H); ^{13}C NMR (CDCl_3 , 125 MHz) δ 21.6, 22.0, 44.3, 47.5, 116.1, 119.9, 126.4, 128.7, 128.9, 129.1, 130.3, 135.7, 135.9, 140.2, 144.6, 155.0, 163.1; IR ν_{CO} (CHCl_3) 1674.4 cm^{-1} ; HRMS (EI) calcd for $\text{C}_{21}\text{H}_{21}\text{N}_1\text{O}_3\text{S}_1$ (M^+) 367.1242, found 367.1244.

X-ray Structures of 13 and 32. Single crystals of compounds **13** and **32** were grown by slow evaporation of CH_2Cl_2 and THF solutions. Diffraction data were collected on an Enraf-Nonius CCD single crystal X-ray diffractometer at room temperature, using graphite-monochromated Mo $\text{K}\alpha$ radiation ($\lambda = 0.71073 \text{\AA}$). Preliminary orientation matrices and unit cell parameters were obtained from the peaks of the first 10 frames and then refined by using the whole data set. Frames were integrated and corrected for Lorentz and polarization effects by using DENZO. Structures were solved by direct methods with use of SHELXS-97⁴⁶ and refined by full-matrix least-squares with SHELXL-97.⁴⁷ All non-hydrogen atoms were refined anisotropically and hydrogen atoms except some were treated as idealized contributions.

Crystal data for **13**: $\text{C}_{20.5}\text{H}_{20}\text{Cl}_1\text{N}_1\text{O}_3\text{S}_1$ (295 K); $M = 389.898$, monoclinic, space group $C2/c$, $a = 26.8036(7) \text{\AA}$, $b = 6.1821(2) \text{\AA}$, $c = 24.8527(8) \text{\AA}$, $\beta = 110.146(2)^\circ$, $V = 3866.2(2) \text{\AA}^3$, $Z = 8$,

(46) Sheldrick, G. M. *Program for the Solution of Crystal Structure*; University of Gottingen: Gottinger, Germany, 1997.

(47) Sheldrick, G. M. *Program for Crystal Structure Refinement*; University of Gottingen: Gottinger, Germany, 1997.

$\rho_{\text{calcd}} = 1.360 \text{ g/cm}^{-3}$, absorption coefficient = 0.326 mm^{-1} , total reflections collected 7514, unique 4360 ($R_{\text{int}} = 0.0261$), GOF = 1.043, $R_I = 0.0466$, $R_w = 0.1116$ ($I > 2\sigma(I)$).

Crystal data for **32**: $\text{C}_{46}\text{H}_{50}\text{N}_2\text{O}_7\text{S}_2$ (295 K); $M = 807.00$, triclinic, space group $P\bar{1}$, $a = 6.3711(3) \text{\AA}$, $b = 13.0727(6) \text{\AA}$, $c = 13.8394(5) \text{\AA}$, $\alpha = 66.842(2)^\circ$, $\beta = 79.983(3)^\circ$, $\gamma = 83.492(2)^\circ$, $V = 1042.33(8) \text{\AA}^3$, $Z = 1$, $\rho_{\text{calcd}} = 1.286 \text{ g/cm}^{-3}$, absorption coefficient = 0.181 mm^{-1} , total reflections collected 7213, unique 7213 ($R_{\text{int}} = 0.0000$), GOF = 1.044, $R_I = 0.0517$, $R_w = 0.1370$ ($I > 2\sigma(I)$). A disordered THF molecule was observed in difference Fourier maps and refined as occupying two positions. All atoms of the THF molecules were isotropically treated, and C–C and C–O bond lengths of the THF molecule were idealized by using the 1,2-distance constraint “DFIX 1.54” and “DFIX 1.40”, respectively. The hydrogen atoms were assigned to idealized positions and were allowed to ride.

CCDC reference numbers CCDC-716233 (**13**) and CCDC-716234 (**32**) contain the supplementary crystallographic data for this paper. These data can be obtained free of charge from The Cambridge Crystallographic Data Centre via www.ccdc.cam.ac.uk/data_request/cif.

Computational Method. The calculations were performed with the Gaussian 03 program package.⁴⁸ In the computational model, the PPh_3 ligand was represented by PH_3 . The tosyl group at the nitrogen atom in the amide-tethered 1,6-eyne substrate was replaced with H. All the results were obtained at the DFT level of theory, using the B3LYP hybrid functional.^{49–51} The gold atom was described by using the LANL2DZ basis set, which includes the relativistic effective core potential (ECP) of Hay and Wadt^{52–54} for the inner electrons and a double- ζ basis set for the outer electrons. The standard 6-31G(d) basis set was used for the remaining atoms. All geometries of stationary states were fully optimized without any symmetry restriction. Frequency calculations were performed to characterize the stationary points as minima or transition states and to obtain the zero-point energies (ZPE) and thermal corrections at 298.15 K. Transition states were identified by using a single negative eigenvalue in the Hessian matrix. Intrinsic reaction coordinate calculations (IRC) were performed to ensure that the transition states actually connect the proposed reactants and products.

Acknowledgment. This work was supported by the Korean Government (MOEHRD) (KRF-2008-341-C00022), and the Korea Science and Engineering Foundation (KOSEF) grant funded by the Korea Government (MEST) (R11-2005-065). Y.T.L. thanks the Brain Korea 21 fellowship and the Seoul Science Fellowship.

Supporting Information Available: Photocopies of ^1H NMR and ^{13}C NMR spectra of all new compounds; ORTEP drawing of comounds **13** and **32**; Cartesian coordinates, energies, and thermodynamic data for all model compounds for computational study; and a complete ref 48. This material is available free of charge via the Internet at <http://pubs.acs.org>.

(48) Frisch, M. J. et al. *Gaussian 03*, Revision C.02; Gaussian, Inc.: Wallingford, CT, 2004. For the full reference, see the SI.

(49) Lee, C. T.; Yang, W. T.; Parr, R. G. *Phys. Rev. B* **1988**, *37*, 785–789.

(50) Becke, A. D. *J. Chem. Phys.* **1993**, *98*, 5648–5652.

(51) Stephens, P. J.; Devlin, F. J.; Chabalowski, C. F.; Frisch, M. J. *J. Phys. Chem.* **1994**, *98*, 11623–11627.

(52) Hay, P. J.; Wadt, W. R. *J. Chem. Phys.* **1985**, *82*, 270–283.

(53) Wadt, W. R.; Hay, P. J. *J. Chem. Phys.* **1985**, *82*, 284–298.

(54) Hay, P. J.; Wadt, W. R. *J. Chem. Phys.* **1985**, *82*, 299–310.